Phase Behavior in Thin Films of Cylinder-Forming Diblock Copolymer: Deformation and Division of Heptacoordinated Microdomains

Karim Aissou,* Thierry Baron, Martin Kogelschatz, and Alina Pascale

LTM/CNRS, CEA/Leti/DTS, 17 Rue des Martyrs, F-38054 Grenoble, France

Received January 5, 2007; Revised Manuscript Received March 21, 2007

ABSTRACT: The microdomain areas in a 2D hexagonal array of vertically oriented PS-*b*-PMMA diblock copolymer cylinders have been studied, and we have found that their area increases as a function of their coordination number. For the 7-fold coordinated cylinders, the unit cell could adopt an anisotropic configuration due to the stress of the lattice. In this case, in order to minimize the free energy of the system, the PMMA domain deforms commensurately with the unit cell and adopts an elliptical or a lozenge-like cross section, in good agreement with strong segregation considerations. However, these strained configurations reveal to be metastable so that thermal fluctuations could induce a transition from a distorted column to two other circular columns. This phenomenon has been used to explain the motion of dislocations.

1. Introduction

Block copolymers self-assembling has been extensively studied in recent years. These periodic microstructures with well-defined size and spacing of tens of nanometers are interesting due to their potential use as deposition or etching masks.[1−6] A simple AB diblock copolymer is composed of fN polymer A segments and of $(1 - f)N$ polymer B segments, linked at one end together by a covalent bond, where N denotes the degree of polymerization and f the fraction of A block in the chain. The product χN controls the tendency of the A and B blocks to separate, where χ is the Flory−Huggins segmental interaction parameter. At sufficiently large values (i.e., $\chi N \geq 10$), the A and B blocks become immiscible and form periodically separated microdomains.[7] Depending on the composition, f, diblock copolymers can organize in several equilibrium structures: lamellae, hexagonally ordered columns, bicontinuous cubic gyroids, or a body-centered-cubic lattice of spheres.[8] The periodicity of these structures is determined by a competition between the interfacial tension and the entropic penalty of stretching of the different blocks in order to maintain a uniform segment density.[9]

Many thin film studies have focused on asymmetric diblock copolymers as nanolithographic templates. These 2D-periodic patterns can be obtained either (1) from a monolayer film organized into close packed spheres or (2) from a thin film containing an array of columns oriented normal to the substrate. Segalman et al.[10] have previously studied the organization of films formed by a monolayer of spheres, and they found that hexagonal block copolymer patterns consist of well-organized areas (grains) separated by boundaries (array of defects) and discrete defects. For these hexagonal phases, dislocations are defined as pairs of columns with five and seven nearest neighbors, respectively. Disclinations are identified as unpaired columns with five or seven neighbors. Recently, Vega and coworkers[11] have noted that disclinations, poorly present in hexagonal patterns, are correlated to high angle grain boundaries (HAGB).

In the literature, Hammond et al.[12] have studied the defect structures of hexagonal patterns of vertically oriented column microdomains. They have shown that columns with 5 or 7 neighbors adjust their diameter (∼area) in response to the stress field associated with the defect. The formation of these defects limits the size of well-organized area. In order to overcome this limitation, macroscopic grain growth in two-dimensional system has been intensively studied during the past decade.[10,11,13,14] For hexagonal patterns of copolymer blocks, it was found that the dominant coarsening process is the collapse of small grains into the grain boundaries of larger grains during thermal annealing.[14] Several mechanisms were proposed to explain this phenomenon: curvature driven grain growth, annihilation of topological defects, and grain rotation.

In this work, by studying the organization of patterns consisting of columns oriented normal to the substrate, we will show that these patterns globally present the same behavior as films with spherical domains. However, in the cylinder pattern case, we note the presence of two types of dislocations with different Burgers vectors. Then, by analyzing the defect sites, we will evidence a disparity of pore areas between 5-fold, 6-fold, and 7-fold coordinated columns, disparity that is higher for the 7-fold sites than for the 5-fold and the 6-fold sites. This strong variation is induced by a deformation of the unit cell from an isotropic hexagon to an anisotropic heptagon. For the 7-fold coordinated cylinders, we will experimentally show that the unit cell could adopt an anisotropic configuration due to the lattice stress. In this case, in order to minimize the free energy of the system, the PMMA domain deforms commensurately with the unit cell and adopts an elliptical or a lozenge-like cross section, well reproduced by strong segregation considerations. In strongly strained configuration, our experimental results will show that thermal fluctuations could overcome the barrier energy, transforming the PMMA distorted columns into two distinct circular columns. Finally, by using the column division phenomenon, a possible mechanism of dislocation diffusion under thermal annealing will be proposed.

2. Experimental Methods

Materials and Film Preparation. To form PMMA cylinders in a PS matrix, we used an asymmetric poly(styrene-*block*-methyl methacrylate) (PS-*b*-PMMA) diblock copolymer from Polymer Source, Inc., having a PMMA weight fraction of 0.3 with a

* Corresponding author. E-mail: karim.aissou@cea.fr.

10.1021/ma070035k CCC: $37.00
Published on Web 06/07/2007

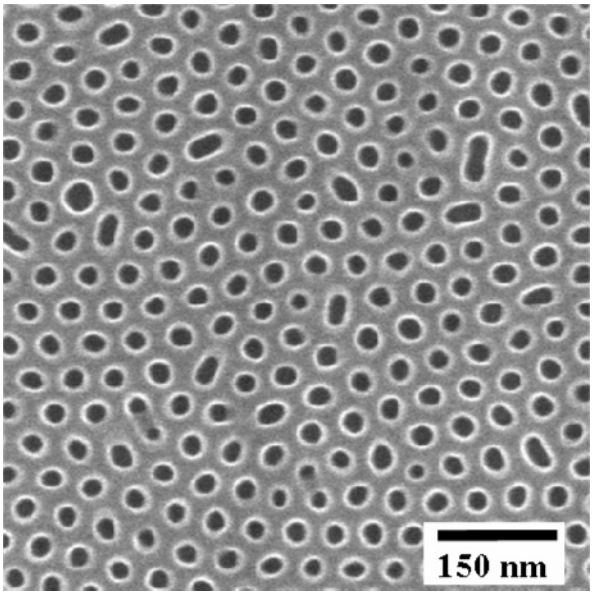

Figure 1. Typical SEM image of a porous PS template film obtained after annealing at 200 °C under vacuum, for 3 days, and after removal of PMMA cylinders.

molecular weight of 67 100 g mol^{-1} and a dispersity of 1.09. The orientation of the cylinder depends on the interaction of the blocks with the substrate. In order to prepare perpendicular PMMA cylinders, the interaction of PS and PMMA blocks with the SiO_2 substrate should be equivalent. This neutralization is obtained by grafting a hydroxy-terminated random copolymer (from Polymer Source, Inc., denoted PS-*ran*-PMMA, with a PS weight fraction of 0.59, M_w of 13 100, and polydispersity of 1.47) on silicon dioxide.[15] Then, a thin film (∼30 nm) of PS-*b*-PMMA was spin-coated from a toluene diluted solution (1% w/w), and samples were annealed at 200 °C for 3 days to promote the organization of the film. Under UV irradiation (HgXe, ∼1.2 J/cm^2) for 15 min, the PMMA phase is degraded via a chain scission and could be removed in acetic acid, whereas the PS was cross-linked and became insoluble, leaving a porous PS template film.

Image Processing and Analysis. The copolymer microstructure was investigated by scanning electron microscopy (Hitachi S5000). Centroid positions and areas of the columns (except those intercepting the border of the image) were analyzed on 1024 nm × 768 nm scans with an image resolution of 640 × 480 pixels. Using this method, the error on the mean surface area covered by the PMMA cylinder is estimated to be less than 5% from an image to another. A Delaunay triangulation mapping of the image is used to determine the cylinder coordination and to visualize the presence of dislocations and disclinations in the system.

3. Results and Discussion

Features of the Patterns. Figure 1 is a SEM image of a typical organization pattern that we obtained after annealing of the PS-*b*-PMMA layer. The film is composed of different grains, in whose columns (dark on the image) are oriented normal to the surface and ordered in a hexagonal array. Each grain presents a specific orientation and is separated of grain boundaries made of dislocations defined as pairs of columns with five (5-fold) and seven (7-fold) nearest neighbors, respectively. The mean maximum Ferret diameter and the mean center-to-center spacing of cylinder are respectively around 20 and 42 nm.

Figure 2 shows a Delaunay triangulation of a typical SEM image. In this figure, we observe the presence of free dislocations and dislocation lines. The dislocations line arises to delimit two grains with a high angle grain boundary (HAGB) (15°−30°) whereas free dislocations induce a low angle grain boundary (LAGB) (0°−15°). The LAGB can be described as a

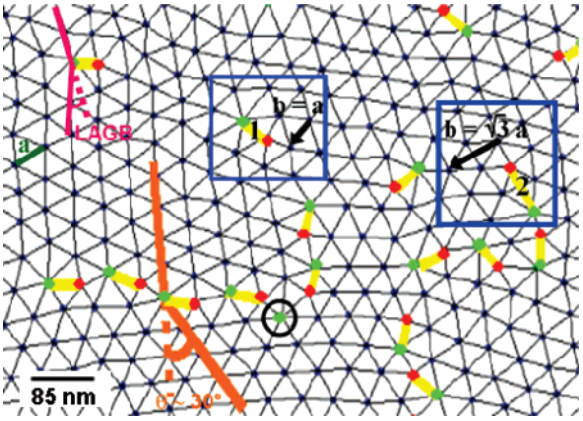

Figure 2. Delaunay triangulation of a porous PS template film obtained under the same conditions as Figure 1. Cylinders with seven neighbors are indicated by green dots, and those with five neighbors are in red. Dislocations formed by a pair of 5−7 disclinations are indicated by a connecting yellow bars. These dislocations could be isolated, and they define a LAGB, or they could be bound to a HAGB. An unpaired disclination bounding to HAGB is indicated by a black circle.The blue rectangles indicate the dislocations of type 1 and 2. Their Burgers vectors, whose directions are indicated by black arrows, have different values.

discrete interface physically punctuated by separated dislocations, which destroy the reference lattice continuity. For LAGB, the dislocation density, d, increases with decreasing angular mismatch as θ/b, where θ is the mismatch in orientation between two adjacent grains and b is the Burgers vector of the interface dislocations. For the HAGB, the dislocation density is not proportional to the angular mismatch. A recent study on the organization of spheres monolayer[10] has reported the same behavior.

In this figure, we have located a disclination with seven neighbors (in the black circle). In the same manner as hexagonal patterns of spherical nanodomains studied by Vega et al.,[11] we always observed that unpaired disclinations, poorly present in the system, are bound to HAGBs.

Finally, we have indicated in rectangles two types of dislocations (1 and 2) with different Burgers vectors, b, whose directions are indicated by black arrows. The type 1 dislocation has a smaller Burgers vector ($b = a$, where a is the lattice constant) than that of type 2 ($b = \sqrt{3}a$). Until there, the presence of type 2 dislocation has never been reported for block copolymer hexagonal patterns. The strain energy of one dislocation, E_d, is proportional to b^2, so type 2 induces a higher strain field in the lattice than type 1 dislocation. It could explain why this configuration is rarely observed in the films and so does not affect the defect shape analysis.

Formation of Distorted 7-fold Coordinated Pores. In this section, we studied the consequence of the lattice stress field on the area and on the shape of cylinders. We will see that these parameters vary as a function of the coordination number.

In SEM images, obtained under the same experimental conditions as Figure 1, we have determined the mean area of 5-fold, 6-fold, and 7-fold coordinated pores. For such sample, the mean surface area of 6-fold sites is centered at 270 nm^2 (σ < 13 nm^2) (Figure 3a). In parts b and c of Figure 3, the pore area distributions for 5- and 7-coordinated columns, evaluated for ∼45−50 sites, are centered at 210−250 and 430−580 nm^2, respectively. Globally, we observed that the mean pore area of columns increases with the coordination number. Hammond and co-workers[12] have previously noted this disparity in size between 5-fold, 6-fold, and 7-fold coordinated columns. The disparity of pore areas is higher for the 7-fold sites than for the 5-fold

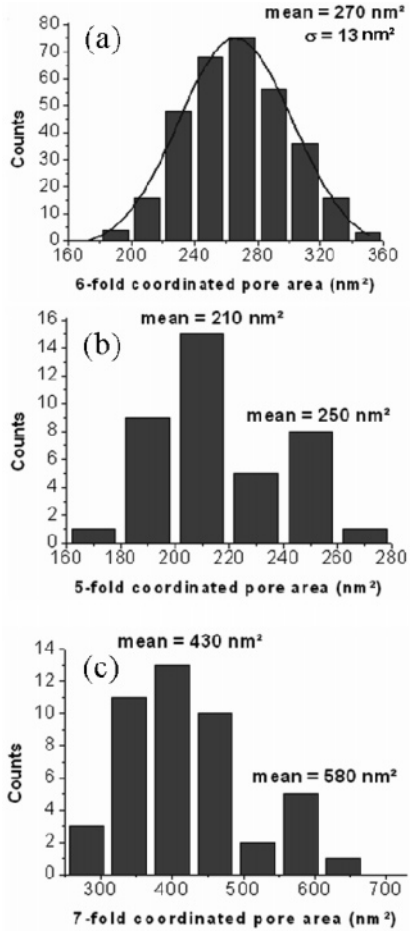

Figure 3. Distributions of the pore areas with different coordination numbers: (a) 6-fold coordinated pores, (b) 5-fold coordinated pores, and (c) 7-fold coordinated pores.

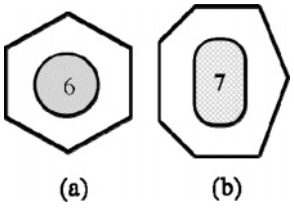

Figure 4. Schematic representations of different unit cells present in the system: (a) an isotropic hexagon with a circular inner core; (b) an anisotropic heptagon with an elliptical or a lozenge-like inner core (represented here).

and the 6-fold sites. This strong variation is due to a deformation of the unit cell from an isotropic hexagon (Figure 4a) to an anisotropic heptagon (Figure 4b). At the same time, the cross section of PMMA columns adopt an elliptical or a lozenge-like shape in order to keep the polymer chain density constant in the unit cell. In the last configuration, the column shape presents flattened sides, parallel to the direction of stretch, and semicircular caps at each end.[16]

As is depicted in Figure 5, the seven coordinated columns could be described as follows: the 7-fold site is always surrounded by five 6-fold and one 5-fold cylinders, whereas the last cylinder is (I) 5-fold, (II) 6-fold, or (III) 7-fold coordinated. As the coordination number of the last cylinder increases from five to seven, the maximum Ferret diameter of domain considered, d_m, and the distance between the centroid cylinder positions of its two farthest neighbors, L, increase.

In order to characterize the deformation of the PMMA cylinder from a circular shape to a lozenge-like shape as a function of the unit cell deformation in the direction of the stress field of the lattice, the dependence of d_m with L/a (where a is the period of the lattice) has been plotted in Figure 6, for the 7-fold defects observed in our samples. We first found that d_m increased with L/a as the environment of the last cylinder increases from five to seven neighbors. Indeed, a higher coordination number increases the strain applied to the unit cell. We also obtained a linear relationship between d_m and L/a, which means that the PMMA microdomain deforms commensurately with the unit cell. By extrapolation for a perfect hexagonal cell (see Figure 6), the value of $d_m = 20.5$ nm is then found corresponding to the experimental value obtained with this kind of diblock copolymers.

To be sure that the cross-section deformation is reflected throughout the whole thickness of the porous PS template, we used it as a mask to generate Si nanopillars (see Figure 7). To obtain these nanopillars we first evaporated a 5 nm layer of Au onto the porous PS pattern. Then, the PS was removed by lift-off, leaving an array of Au dots on the Si substrate which was used as a mask for etching the Si substrate with a Cl_2/O_2 plasma. Figure 7 shows the presence of 7-fold coordinated nanopillars having a distorted shape (surrounded by white circles). The

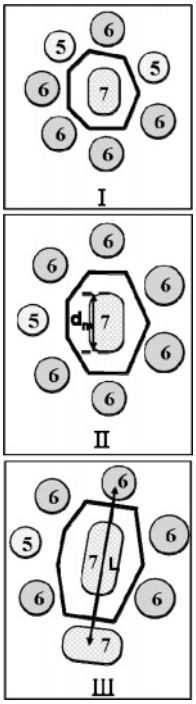

Figure 5. Possible environments of 7-fold defect sites where the number in every pore specifies their degree of coordination. The deformation of 7-fold pore increases from an environment of type I to an environment of type III. d_m indicates the maximum Ferret diameter of the pore, and L gives the distance between the centroid cylinder positions of two farthest neighbors.

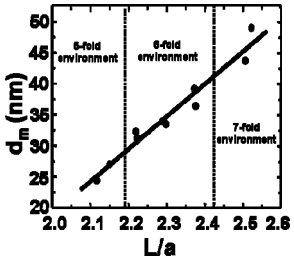

Figure 6. Linear dependence of the maximum Ferret diameter d_m from 7-fold coordinated cylinders on L/a distance. For $L/a = 2$, $d_m = 20.5$ nm, in agreement with experimental observations.

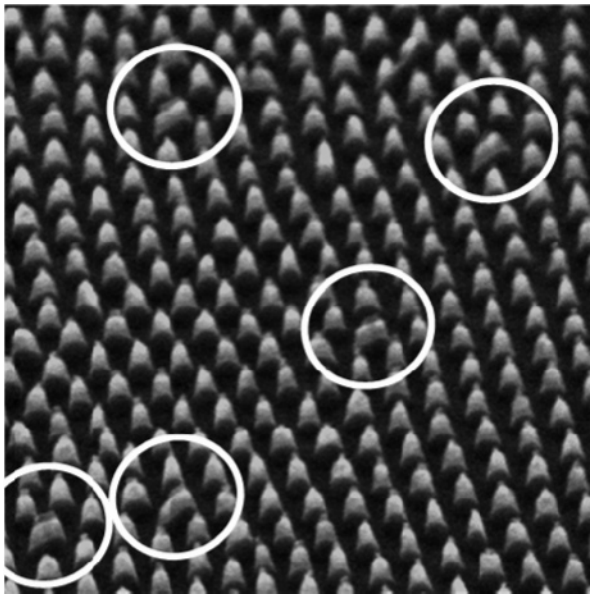

Figure 7. SEM image of an organized silicon nanopillar array obtained by using metallic Au dots as a mask for plasma etching (Cl_2/O_2). 7-fold coordinated nanopillars in white circles present a deformation in direction of its farthest neighbors.

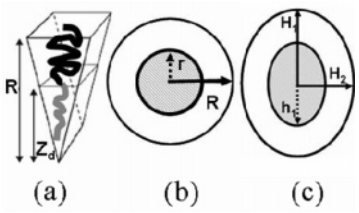

Figure 8. (a) Wedge used for building up cylindrical structures. The height of the wedge is R, and the AB interface is located at height Z_d. Circular (b) and elliptical (c) unit cells used for the Olmsted−Milner calculation.

nanopillar deformation in direction of its farthest neighbors confirms that the distortion is maintained throughout the film thickness.

Energetic Considerations. We will now focus our attention on an energetic consideration of the unit cell in order to explain the 7-fold column distortion. To do this, we will theoretically determine and compare the unit cell free energy for a circular and an elliptical configuration which correspond to an isotropic and an anisotropic strain of the cell (see Figure 8). These two configurations have been chosen to simplify the model and will give a good qualitative description of the phenomenon observed.

In the limit of strong-segregation theory (i.e., $\chi N \rightarrow \infty$), the free energy of a unit cell, F_{cell}, is given by

$$F_{cell} = F_{int} + F_{el,A} + F_{el,B} + F_{surf} \tag{1}$$

where F_{int} is the interfacial surface energy between A and B phases, $F_{el,A}$ and $F_{el,B}$ are the account for the entropic losses due to the stretching of A and B blocks, respectively, and F_{surf} is the surface energy between A and B components and the bounding surface.

We will now evaluate the expression of each term including in the free energy of the unit cell. First, for the two configurations (elliptical and circular) as the substrate surface was neutralized by the deposition of a random copolymer layer prior to the deposition of the diblock copolymer layer, $F_{surf} = 0$ in our conditions.

To estimate the others terms (F_{int}, $F_{el,A}$, $F_{el,B}$), the Olmsted−Milner wedge calculation,[17] which consists of splitting the unit cell into a series of pie-shaped wedges and calculating the energy in each wedge, is used. Then, for the calculation we used the unit cell approximation (UCA), where the isotropic (anisotropic) heptagonal cell (see Figure 4b) is replaced by a circular (elliptical) Wigner−Seitz cell (WS) and a circular (elliptical) AB interface (see Figure 8). Using the Olmsted−Milner calculation is justified as in our case the AB interface deforms commensurately with the unit cell (see Figure 6). We want to point out the fact that the UCA assumption underestimates the free energy of the true morphology, but the qualitative analysis remains valid.

For clarity, we will start with the calculation of F_{cell} for a circular shape, and then we will evaluate F_{cell} for the elliptical shape.

F_{cell} Circular: Isotropic Elongation. Following the Olmsted−Milner method, the volume occupied by the A block relative to the total volume of the wedge must satisfy the local volume constraint which implies that $Z_d/R = f^{1/2}$ for a cylindrical geometry.

The elastic energy in the θ-th wedge, calculated by a method developed for the polymer brushes,[18,19] is given by

$$F_{el,\theta} = \frac{k_B T \pi^2 R_\theta^{\,2}}{48(aN^{1/2})^2 \upsilon_\theta(1)}\left[\frac{I_{A,\theta}}{f^2} + \frac{I_{B,\theta}}{(1-f)^2}\right] \tag{2}$$

where $aN^{1/2}$ is the ideal Gaussian chain end-to-end distance, $\upsilon_\theta(1) = {}^1/_2$, and

$$I_{A,\theta} = 3\int_0^{1-\sqrt{f}} (y + \sqrt{f})\, y^2\, dy \tag{3}$$

$$I_{B,\theta} = 3\int_0^{\sqrt{f}} (\sqrt{f} - y) y^2\, dy \tag{4}$$

The interfacial surface energy in the θ-th wedge is written as $F_{int,\theta} = \gamma_{AB} P(\theta) f^{1/2}$, where γ_{AB} is the surface tension between A and B blocks and $P(\theta)$ is the perimeter length of the this wedge.

The total free energy of the θ-th wedge is $F_\theta = F_{int,\theta} + F_{el,\theta}$, and the free energy of the cell, when $\theta \rightarrow 0$, is just $F_{cell} = \int_{cell} F_\theta / \int_{cell} d\upsilon_\theta$, where $d\upsilon_\theta$ is the volume of the θ-th wedge.

The optimal radius, R^*, is given by

$$R^* = \left[\frac{96(\gamma_{AB} a^2/k_B T) N^2 \nu}{\pi^2} \frac{f^{1/2}}{[1 + (1-f^{1/2})^3 (3 + f^{1/2})/(1-f)^2]}\right]^{1/3} \tag{5}$$

and the optimal free energy, F^* (without lattice stress), per unit volume is given by

$$F^* = \frac{k_B T}{N\nu}\left(\frac{27\pi^2}{96}\right)^{1/3}\left(\frac{\gamma_{AB} a^2}{k_B T}\right)^{2/3}\left(\frac{\nu^{1/3}}{a}\right)^2 N^{1/3}\left[f + \frac{f(1-f^{1/2})^3(3+f^{1/2})}{(1-f)^2}\right]^{1/3} \tag{6}$$

where ν is the monomer volume.

Consequently, the free energy of a circular unit cell for any R can be trivially written as

$$F_{circular} = \frac{F^*}{3}\left[\left(2\frac{R^*}{R}\right) + \left(\frac{R}{R^*}\right)^2\right] \tag{7}$$

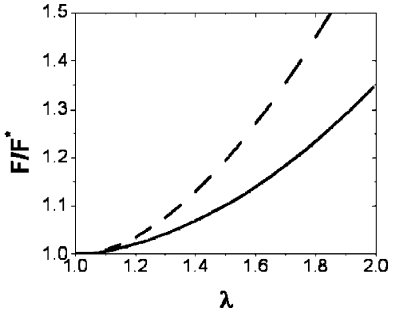

Figure 9. Free energy comparison of a circular (dashed curve) and an elliptical (full curve) unit cell geometry as a function of $\lambda \equiv R/R^* \equiv H_1/R^*$.

F_{cell} Elliptical: Anisotropic Elongation. By contrast to the circular configuration, for the elliptical distortion the radius and surface area change for each wedge. To take into account this modification, Pereira[20] considers an ellipse with a semimajor axis H_1 and a semiminor axis H_2 so that the eccentricity e is defined by

$$e^2 = 1 - (H_2/H_1) \tag{8}$$

Thus, Pereira finds that the interfacial energy is given by

$$F_{\text{int}} = 4\gamma_{\text{AB}} f^{1/2} H_1 (1-e^2)^{1/2} \int_0^{\pi/2} \left(1 - \frac{e^2}{e^2-1}\sin^2\theta\right) \mathrm{d}\theta \tag{9}$$

whereas the total stretching energy is given by

$$F_{\text{el}} = \frac{k_{\text{B}} T \pi^2}{32 N v} H_1^4 \left[\frac{1}{6Na^2} + \frac{(1-f^{1/2})^3(3+f^{1/2})}{6Na^2(1-f)^2}\right](1-e^2)^{1/2} I(e^2) \tag{10}$$

where

$$I(e^2) = (1-e^2)^{3/2} \times \int_0^{\pi/2} \frac{[1+e^4\cos^2\theta\sin^2\theta/(1-e^2\cos^2\theta)^2]^{1/2}[\sin^2\theta + (1-e^2)\cos^2\theta]}{(1-e^2\cos^2\theta)^2[\sin^2\theta+(1-e^2)\cos^2\theta]^{1/2}} \mathrm{d}\theta \tag{11}$$

The free energy per unit volume, for the elliptical state, is

$$F_{\text{elliptical}} = \frac{2F^*}{3\lambda}\frac{2}{\pi}\int_0^{\pi/2}\left(1 - \frac{e^2}{e^2-1}\sin^2\theta\right)\mathrm{d}\theta + \frac{F^*}{3}\lambda^2\frac{2}{\pi}I(e^2) \tag{12}$$

where $\lambda \equiv H_1/R^*$ is the strain of the cell. The free energy for any λ is determining by minimizing $F_{\text{elliptical}}$ with respect to e.

In Figure 9, the dimensionless free energy ratios (F_{circular}/F^* and $F_{\text{elliptical}}/F^*$) are plotted as a function of $\lambda \equiv H_1/R^* \equiv R/R^*$. In absence of the deformation ($\lambda = 1$), a circular cell is more stable than an elliptical one. For $\lambda > 1$, the elliptical configuration minimizes the free energy of the system. From these results, we conclude that the unit cell adopts an anisotropic configuration to decrease its free energy when the stress of the lattice induces a large strain of the cell. This is in a good agreement with our experimental results. Indeed, a circular PMMA cylinder is observed for a small deformation of the unit cell (i.e., for a pore having an environment of type I) (5-fold), whereas an anisotropic shape is observed for pores having an environment of type II (6-fold) or III (7-fold). Experimentally, in the case of a large lattice stress λ (>1.6), the configuration of the cell is rather a lozenge than an ellipse, and this imposes a lozenge shape for the cylinders.

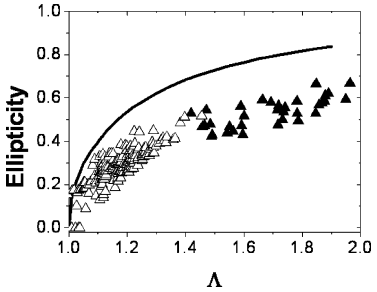

Figure 10. Ellipticity comparison of 7-fold (full triangles) and 6-fold (empty triangles) coordinated columns as a function of $\Lambda \equiv h_1/r^*$. Theoretical ellipticity values which minimize the free energy for a given strain of the cell are shown on the full curve.

In Figure 10, we have plotted the experimental and the theoretical cylinder ellipticity, e (see eq 8), as a function of the column strain, Λ. For the experimental results, Λ is defined as the ratio of the semimajor axis of the column, h_1, to the optimal mean radius of hexacoordinated cylinders, r^*. To obtain the optimal theoretical ellipticity of the strained column ($\Lambda > 1$), we must replaced λ by Λ in the eq 12 (since $\Lambda \equiv h_1/r^* \equiv \sqrt{f}H_1/\sqrt{f}R^* \equiv \lambda$) and then minimized this equation for a particular Λ. We first found that Λ is generally stronger for 7-fold coordinated columns (full triangles) than 6-fold coordinated ones (empty triangles) which correspond to a higher distortion of the cylinder to minimize the free energy of the cell. We mention that cylinder distortions (ellipticity) are generally smaller than the theoretical ones (full curve). From these results, we conclude that theoretical and experimental plots exhibit the same behavior attesting that the column is elliptically deformed when the cell is strained. However, the theoretical deformation is never obtained because the Milner−Olmsted wedge approach upper estimates the real behavior of the cell.

Division of Distorted 7-fold Coordinated Pores. The presence of distorted PMMA domain in the system is a result of the stress field of the lattice. In this section, we will see that local thermal random fluctuations could affect the stability of distorted column.

For the 7-fold coordinated columns presenting a lozenge-like cross section, we often observe the presence of a pinched side instead of a flattened side. The pinched side forms preferentially in the proximity of the 5-fold coordinated neighbor column (Figure 10a). In Figure 10a, we show that the second side could be pinched depending on the position of others neighbors. As it was proposed by Matsen[21] for the cylinder−sphere transition, we expect that the domain division is nucleated when the cylinder is pinch off. After this irreversible step, ruptures occur in both directions transforming the distorted domain into two cylinders. In Figure 11b, we have quenched a 7-fold coordinated column being divided into two other columns. On this SEM image, we can see a dark trail between separated columns, which corresponds to the PMMA removed during the UV treatment. Thus, when the energy barrier, ΔE, between the two equilibrium phases is overcome by thermal fluctuations, divided domains move to adjust their domain spacing with the equilibrium periodicity. Resulting columns present a circular shape with five and six neighbors (see Figure 11b).

Proposed Mechanism of Dislocation Diffusion. Although progress has been made to understand the coarsening process, there are still many open questions concerning the basic mechanisms leading the dislocation diffusion for such systems.

In Figure 12, we propose a possible mechanism of dislocation diffusion via column divisions from extrapolations of a SEM image (schematized in Figure 12b). Figure 12a shows three

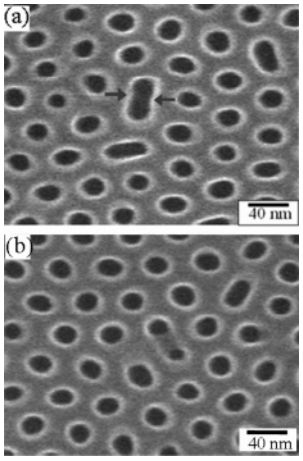

Figure 11. SEM images: (a) A 7-fold coordinated site with an environment of type III. Parallel to the direction of stretch, pinching are indicated by arrows. (b) A 7-fold coordinated site which splits into two others columns and allowing the formation of PMMA chains between the new domains.

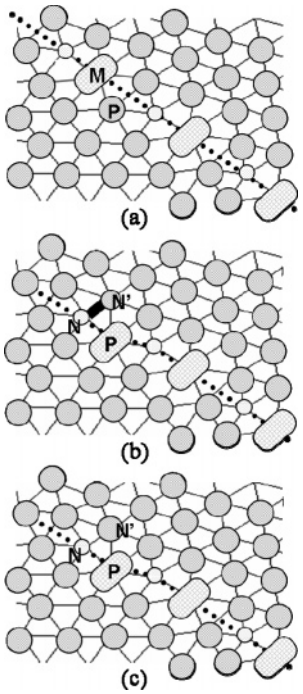

Figure 12. Schematic representation illustrating the displacement of a dislocation in the pattern: (a) Before the division, the grain boundary (dotted line) is linear. (b) The heptacoordinated domain, noted *M*, is dividing into two domains noted *N* and *N*′, having five and seven neighbors, respectively. (c) After the division the dislocation is composed by paired domains, noted *N* and *P*, which induce a displacement of the grain boundary.

dislocations delimiting a linear grain boundary (dotted line) before the 7-fold coordinated column noticed *M* divides. At this stage, its AB interface has a lozenge-like cross section. We have also labeled a 6-fold coordinated column with the letter *P*. In Figure 12b, column *M* is splitting and two domains noted *N* and *N*′ are formed. These new columns are located on both sides from the original grain boundary, leaving a typical trail of PMMA block in the PS matrix (phenomenon observed in Figure 12b). In the new organization of the pattern, *N* and *N*′ have five and six neighbors, respectively, whereas *P* is now hepta-coordinated. The distortion of the *P* cell induces a lozenge-like cross section of the PMMA interface to minimize its free energy. In Figure 12c, the pattern at the end of the domain division is presented: the remaining PMMA coming from the previous trail has diffused to complete *N*′ and *N* at their equilibrium position. Following this mechanism, we show that the domain division induces a displacement and a new orientation of the dislocation. Sometimes, this phenomenon, described here for one dislocation, could be observed for all the dislocations bound to the same grain boundary. More generally, we suppose that the domain division mechanism could be a basic model to understand more complicated phenomenon happening in any kind of hexagonal block copolymer systems such as annihilation of topological defects, curvature driven grain growth, and grain rotation.

4. Summary

The study of a 2D hexagonal array of vertically oriented PS-*b*-PMMA diblock copolymer cylinders shows that the cylinder area depends on the environment of their neighbors. Thus, for the 7-fold coordinated cylinders, we have found experimentally and theoretically that the PMMA interface could adopt a lozenge like cross section. Afterward, we have proven that the PMMA interface deforms commensurately with the unit cell, allowing the system free energy minimization. However, the barrier energy which stabilizes the distorted configuration could be overcome by thermal fluctuations. In this case, the PMMA domain splits in order to generate two distinct circular domains. This phenomenon was employed to explain the motion of dislocations.

Acknowledgment. We are grateful to T. Fournier from CRTBT-CNRS and P. Gentile from CEA-Grenoble for their technical assistance as well as to the platform of CEA-LETI for technological support.

References and Notes

(1) Black, C. T.; Guarini, K. W.; Milkove, K. R.; Baker, S. M.; Russell, T. P.; Tuominen, M. T. *Appl. Phys. Lett.* **2001**, *79*, 409.
(2) Cheng, J. Y.; Ross, C. A.; Chan, V. Z-H.; Thomas, E. L.; Lammertink, R. G. H.; Vancso, G. J. *Adv. Mater.* **2001**, *13*, 1174.
(3) Guarini, K. W.; Black, C. T.; Zhang, Y.; Kim, H.; Sikorski, E. M.; Babich, I. V. *J. Vac. Sci. Technol. B* **2002**, *20*, 2788.
(4) Park, M.; Chaikin, P. M.; Register, R. A.; Adamson, D. H. *Appl. Phys. Lett.* **2001**, *79*, 257.
(5) Koslowski, B.; Strobel, S.; Herzog, T.; Boyen, H. G.; Notz, R.; Ziemann, P.; Spatz, J. P.; Moller, M. *J. Appl. Phys.* **2000**, *87*, 7533.
(6) Lammertink, R. G. H.; Hempenius, M. A.; Chan, V. Z-H.; Thomas, E. L.; Vancso, G. J. *Chem. Mater.* **2001**, *13*, 429.
(7) Ohta, T.; Kawasaki, K. *Macromolecules* **1986**, *192*, 621.
(8) Matsen, M. W.; Schick, M. *Phys. Rev. Lett.* **1994**, *72*, 2660.
(9) Matsen, M. W.; Bates, F. W. *Macromolecules* **1996**, *29*, 7641.
(10) Segalman, R. A.; Hexemer, A.; Hayward, R. C.; Kramer, E. J. *Macromolecules* **2003**, *36*, 3272.
(11) Vega, D. A.; Harrison, C.; Angelescu, D. E.; Trawick, M. L.; Huse, D. A.; Chaikin, P. M.; Register, R. A. *Phys. Rev. E* **2005**, *71*, 061803.
(12) Hammond, M. R.; Sides, S. W.; Fredrickson, G. H.; Kramer, E. J.; Ruokolainen, J.; Hahn, S. F. *Macromolecules* **2003**, *36*, 8712.
(13) Pignol, R. J.; Gomez, L. R.; Bast, W.; Vega, D. A. *Physica B* **2004**, *67*, 800.
(14) Harrison, C. K.; Angelescu, D. E.; Trawick, M. L.; Cheng, Z.; Huse, D. A.; Chaikin, P. M.; Vega, D. A.; Sebastian, J. M.; Register, A.; Adamson, D. H. *Europhys. Lett.* **2004**, *67*, 800.
(15) Mansky, P.; Liu, Y.; Huang, E.; Russell, T. P.; Hawker, C. *Science* **1997**, *275*, 1458.
(16) Pereira, G. G. *Eur. Phys. J. E* **2002**, *7*, 273.
(17) Olmsted, P. D.; Milner, S. T. *Macromolecules* **1998**, *31*, 4011.
(18) Semenov, A. N. *JETP* **1985**, *88*, 1242.
(19) Milner, S. T.; Witten, T. A.; Cates, M. E. *Macromolecules* **1988**, *21*, 2610.
(20) Pereira, G. G. *J. Chem. Phys.* **2001**, *117*, 1878.
(21) Matsen, M. W. *J. Chem. Phys.* **2001**, *114*, 8165.

MA070035K